Environmental Earth Sciences (2024) 83:352
https://doi.org/10.1007/s12665-024-11653-8

ORIGINAL ARTICLE

Centrifuge modeling of intact clayey loess slope by rainfall

Changyu Liang[1] · **Shuren Wu**[1]

Received: 25 June 2023 / Accepted: 5 May 2024 / Published online: 21 May 2024

Abstract
Loess area is the region that geohazards happened most frequently, accounting for 1/3 of the geohazards in China. Cutting slope has become the most prominent products in human engineering activities and slope failure induced by rainfall has become the main form in recent years. Well-instrumented centrifuge model tests have been introduced to investigate the failure process and failure pattern, including pore water pressure, progressive deformation-failure process and characteristic of the high cutting slope by rainfall. The results show that rainfall induced loess slope failure is characterized by shallow slide to flow and two deeper creepage sliding-tension surfaces. All the sliding faces are characterized by planar surfaces parallel to slope surface. The planar sliding surface differs a lot to the circular sliding surface in the gravitational soil landslide. The accumulative deformation especially the abrupt displacement before failure induced the excess pore water pressure, after which flow failure with high-speed happened. The pore-water transducers on both sides of the shallow sliding surface have distinct response to slope deformation. The quantitative monitoring data indicates that the liquefaction is not the reason but the result of the deformation accumulation and big transient deformation.

Keywords Intact clayey loess · Rainfall · Slide-flow · Planar sliding · Progressive deformation-failure process · Centrifuge model test

Introduction

The loess area in China is 6.3×10^5 km^2, accounting for about 6.6% of China's land area. Because of the big thickness, loose structure, wide distribution of gully and ravine, and the big difference in terrain elevation in loess area, with the concentrated rainfall in certain months, the geoenvironment is very fragile. Loess area has become the region in which geohazards happened most frequently, up to 1/3 of the geohazards in China (Peng et al. 2014). In recent years, with the development of urbanization process and the implementation of the strategy of western development, loess slope (man-made slope, such as road or highway slope, canal slope and cave slope) has become the most prominent products in human engineering activities, in which cutting slope is the main form. Owing to the close relationship with the lifeline engineering, the disaster would have significant amplification effect once slope failure happens (Wu et al. 2013).

✉ Changyu Liang
23598252@qq.com

[1] Institute of Geomechanics, Chinese Academy of Geological Sciences, Beijing 100081, People's Republic of China

In recent years, the frequency, precipitation and duration of extreme rainfall have significantly increased (Huang et al. 2014). Shallow loess landslides induced by rainfall are very common in the Loess Plateau, not only in sandy loess area and typical loess area, but also in clayey loess area; and they usually cause great harm to life and property. Flood season in Yan'an city in July 2013 was characterized by group happening of geological disasters and the number was up to 8135, during which 45 people were killed (Wang et al. 2015). Continuous heavy rainfall from 20 June to 25 July 2013 induced a large number of shallow landslides and debris flows in southern Tianshui, China, resulting in 24 deaths, one missing person and 2386 collapsed houses (Qi et al. 2021). From July to October 2011, concentrated heavy rainfall induced 1200 shallow landslides, which resulted in a total of 7 casualties (Xin et al. 2015).

In terms of research on rainfall-induced shallow landslides, many explorations to hydraulic responses, the characteristics and mechanism of failure have been carried out. The methods mainly include numerical modeling (Egeli and Pulat 2011; Ng and Shi 1998; Gavin and Xue 2008; Oh and Lu 2015; Li et al. 2013; Cascini et al. 2013; Wu et al. 2017; Sun et al. 2021), field test (Ochiai et al. 2004; Tu et al. 2009; Sorbino and

Nicotera 2013; Lim et al. 1996; Sun et al. 2021) and physical modeling test (Take and Bolton 2002; Take et al. 2004; Tohari et al. 2007; Ling et al. 2008; Wang et al. 2010, 2021a; Zhang et al. 2012; Ling and Ling 2012; Hakro and Harahap 2015; Mohammad et al. 2017; Wu et al. 2017). Through a single layered infinite model, Li et al. (2013) found that the propagation of wetting front control the depth of failure plane. Oh and Lu (2015) expanded the traditional limit equilibrium and finite element methods to unsaturated conditions using a generalized effective stress framework and found that the actual failure occurred when the simulated factor of safety approaches its minimum below 1.0. Gavin and Xue (2008) proposed an infiltration model based on the Green-Ampt model and indicated that the infiltration rate is controlled by the permeability of the soil. Ng and Pang (2000) suggested that for the cut slope and the rainfall considered, the wetting stress-dependent soil–water characteristic curves should be considered. Through the research on the CL-ML type soil, Egeli and pulat (2011) found that all 35° slopes were failure by translational failure and for low degrees of saturation, menisci presence and suction effects govern shear strength behavior. The changes in matric suction and pore water pressure caused by rainfall infiltration are the focus of field experiments. It is generally believed that a decrease in matric suction can induce shallow landslides, and the initiation of landslides is generally related to a sudden increase in pore water pressure or the development of perched water tables (Ochiai et al. 2004; Tu et al. 2009; Sorbino and Nicotera 2013; Lim et al. 1996). Based on the highly instrumented centrifuge model test, Take et al. (2004) found that high-speed failures with low angle run-outs are easily triggered in model fill slopes from initially slow moving slips driven by localized transient pore water pressure arising from constricted seepage and material layering. Tohari et al. (2007) indicated that the hydrologic response forms the basis for the development pf a prediction methodology for rainfall-induced failure. Centrifuge modeling of sand (sand-mixtures) slope instability showed that the instability of slopes during rainfall was due to a loss of matric suction that is equivalent to reduction in apparent cohesion and the circular mechanism was confirmed to be validated (Ling et al. 2008; Ling and Ling 2012). The deformation-failure behavior could be influenced by cracks or weak layer during rainfall (Wang et al. 2010; Zhang et al. 2012). Through model flume, Hakro and Harahap (2015) found that slope failure occurred due to increase in moisture content and rise in pore pressure and measurements of moisture content may be more reliable for early warning of slope failure. The flume tests on clean fine sand indicated that the failure surfaces are mostly translational and the failure mechanism is infinite-slope type landslide, highlighting the role of wetting front or matric suction (Mohammad et al. 2017). The above research mainly focuses on water infiltration regularities and the process of failure initiation to clarify the underlying triggering mechanism of rainfall-induced shallow landslides, which deepen our understanding of this type of landslides.

However, although rainfall has been considered as a key role in slope instability in loess platform (Wang et al. 2015; Dijkstra et al. 1994; Sun et al. 2021), now only a few reports (Wang et al. 2015; Wu et al. 2017; Sun et al. 2021) are about loess slope by rainfall. The existing studies focus on field tests (Xu et al. 2013; Li et al. 2014; Sun et al. 2021) and reduced-scale model tests (Chen et al. 2013; Wang et al. 2009; Wu et al. 2017), which mainly focused on the infiltration regularities. There is still lack of well-instrumented and documented physical models especially model tests at the prototype scale such centrifuge tests for the development and validation of some numerical model to reveal the nature of loess slope failure initiation and motivation. Furthermore, considering the wide distribution of loess in China and the wide and frequent development of avalanches and landslide induced by rainfall, it is worthy to carry out in-depth discussion and research on slope deformation-failure process and its mechanism by rainfall. Meanwhile, in view of the special structure (include its cementation, big pores and numerous micro–macro joints) and mechanical properties (such that cutting slopes with angles in excess of the critical state friction angle are common) of loess, it is of great practical significance to do researches by using intact loess sample. But until now there is none report about intact especially large intact loess block investigated in model tests at lab, which might be mainly because of the great difficulty, big cost and time consuming of obtaining big block of loess sample from the field.

This work aims to explore and analyze the underlying mechanism of the shallow clayey loess landslides induced by rainfall quantitatively through a well-instrumented centrifuge model test. The rainfall infiltration regularities, pore pressure characteristics, the deformation-failure process of intact clayey loess would be reported and analyzed. The test was carried out on the geotechnical centrifuge at Hong Kong University of Science and Technology (HKUST). The slope model was constructed to simulate the cutting slope, with the ultimate height of 30 m. Based on the results, the pore water pressure characteristics, vertical displacement of the slope, the deformation-failure process, failure pattern and the mechanism of the slope were analyzed. Except the special instructions, all the data or analysis in this paper is based on the model scale.

Sample collecting and soil properties

Later Pleistocene intact loess block measuring 420 mm × 600 mm × 720 mm were obtained from the top of the Loess Plateau in Baoji (Fig. 1). Then, the sealed samples were placed into wooden boxes with quakeproof

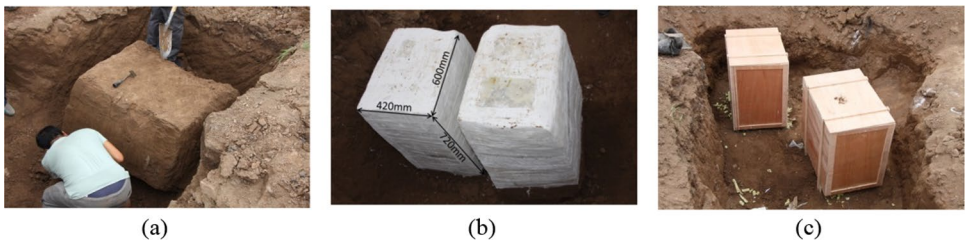

Fig. 1 Sampling in field **a** sampling; **b** intact loess sample sealed with wax; **c** binning

Table 1 Physical properties of loess used in this study

Physical property	Value
Sand (%)	6.00
Silt (%)	74.00
Clay (≤0.002 mm) (%)	20.00
Clay (≤0.005 mm) (%)	28.00
Initial moist bulk density (g/cm^3)	1.67
Natural moisture content (%)	18.84
Liquid limit (%) (10 mm)	33.53
Plastic limit (%) (10 mm)	20.80
PI (%)	12.73
Saturated permeability coefficient (10^{-6} m/s)	3.60

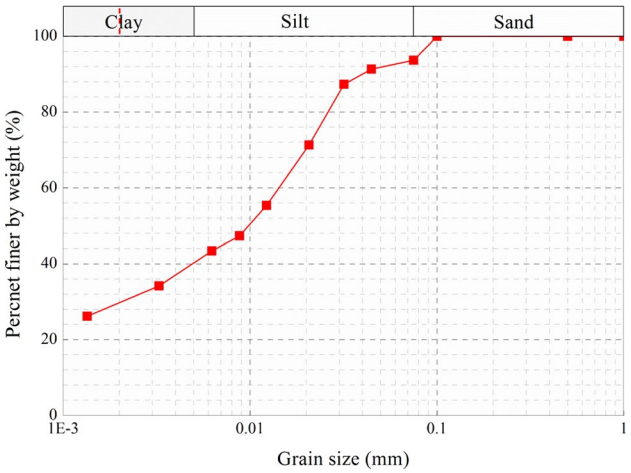

Fig. 2 Loess particle size distribution

cystosepiment (Fig. 1c) and transported to the laboratory at HKUST. Table 1 summarizes the basic physical properties of the studied loess in Baoji, which were determined following the Chinese standards of Ministry of Construction (GB/T50123, 2019). Figure 2 shows the loess particle size distribution. More details can be seen in the previous research by Liang et al. (2018).

Centrifuge model test

Centrifuge at HKUST

The model tests were performed on the geotechnical centrifuge established at HKUST, with a rotating arm of approximately 8 m in diameter and the maximum modeling capacity of 400 g-ton (Fig. 3). A model of reduced size (n time smaller than full scale) may be used to simulate the full-scale slope by increasing the acceleration to n times gravity, namely the model slope would achieve the same stress–strain environment as the prototype slope. The scaling laws of centrifuge modeling have been well established. The time scale for the rainfall event was also reduced by n in the centrifuge. Major scale factors in terms of model values divided by prototype values involved in this article can be derived as shown in Table 2. The model slope of 500 mm high was simulated, the target g level was 60 g, and the rainfall intensity was 13 mm/h. The extreme case of slope failure by rainfall would be simulated, so the rainfall would be applied until slope failure, which needs the water chamber supplying rainfall continuously.

Fig. 3 Geotechnical centrifuge at HKUST

Rainfall system

The centrifuge is instrumented with an in-flight rainfall system which consists of water chamber and spray nozzles (Fig. 4). Water is supplied via water tube by hydraulic pump outside centrifuge machine. The pump provides water pressure of 55 kPa which is equivalent to pressure for tap water in Hong Kong. Water chamber provides an air-tight

Table 2 Relevant scaling laws to this study (after Taylor 1995)

Types	Physical quantity	Unit	Scale factor (model/prototype)	Note
Physical dimensions	Length (l)	m	1/n	n = 20,40,50,60
	Displacement(s)	m	1/n	
Material characteristics	Density(ρ)	kg/m^3	1	
	Mass	kg	1/n^3	
	Unit weight(γ)	N/m^3	n	
	Cohesion(*c*)	Pa	1	
	Internal friction angle (φ)	°	1	
	Stress (p)	N/m^2	1	
	Strain (ε)	–	1	
Rainfall	Time (seepage)	s	1/n^2	
	Pore fluid velocity	m/s	n	
	Rainfall intensity	m/s	n	

environment so that the water pressure can be raised up to the target pressure and the fixed rainfall intensity can be guaranteed.

Water chamber can supply water throughout the test through two-way valve control of the water way and air path: first couple for water (W_I and W_O) and another couple for air(A_I and A_O). The water is pressured when valve A_I is open and A_O and W_I are closed. If water is needed, air pressure must be released before adding water to water chamber. A_I is then closed, while A_O and W_I is now open. The operation of rainfall is controlled by valve W_O which is connected to spray nozzles. All 6 nozzles are LNN-1/4 hydraulic atomizing spray nozzles and brought from Spraying System and Co. with small orifice diameter of 0.51 mm. The drops achieve misting performance and this can minimize Coriolis effect. The nozzles are installed vertically downward to assure an adequate distribution of droplets covering soil area of 585 mm-length and 350 mm-width. The rainfall intensity is calibrated between amount of water measured from nozzle and applied pressure. As the flow rate is controlled by applied air pressure, the effect of elevated gravity on water flow is not significant.

Slope geometry and boundary conditions

Figure 5 shows the elevation and plane view of the model slope and the elevation and plane view of the rainfall nozzle distribution. The nozzles are installed vertically downward to assure an adequate distribution of droplets covering soil area. The model container has internal dimensions of 1245 mm in length, 350 mm in width and 851 mm in height. The inclination angle of the model slope is 52°, which is typical among cutting slopes in Baoji. The model slope height

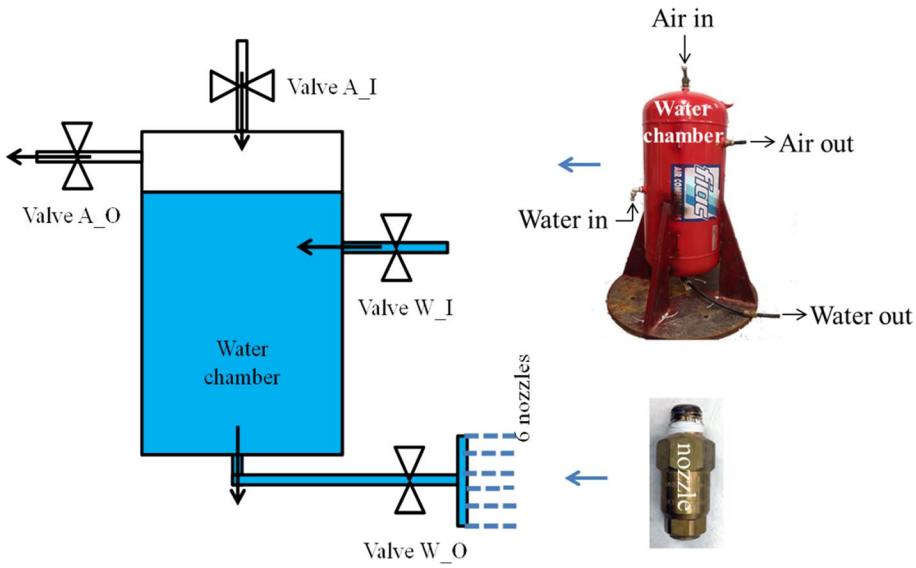

Fig. 4 In-flight rainfall system

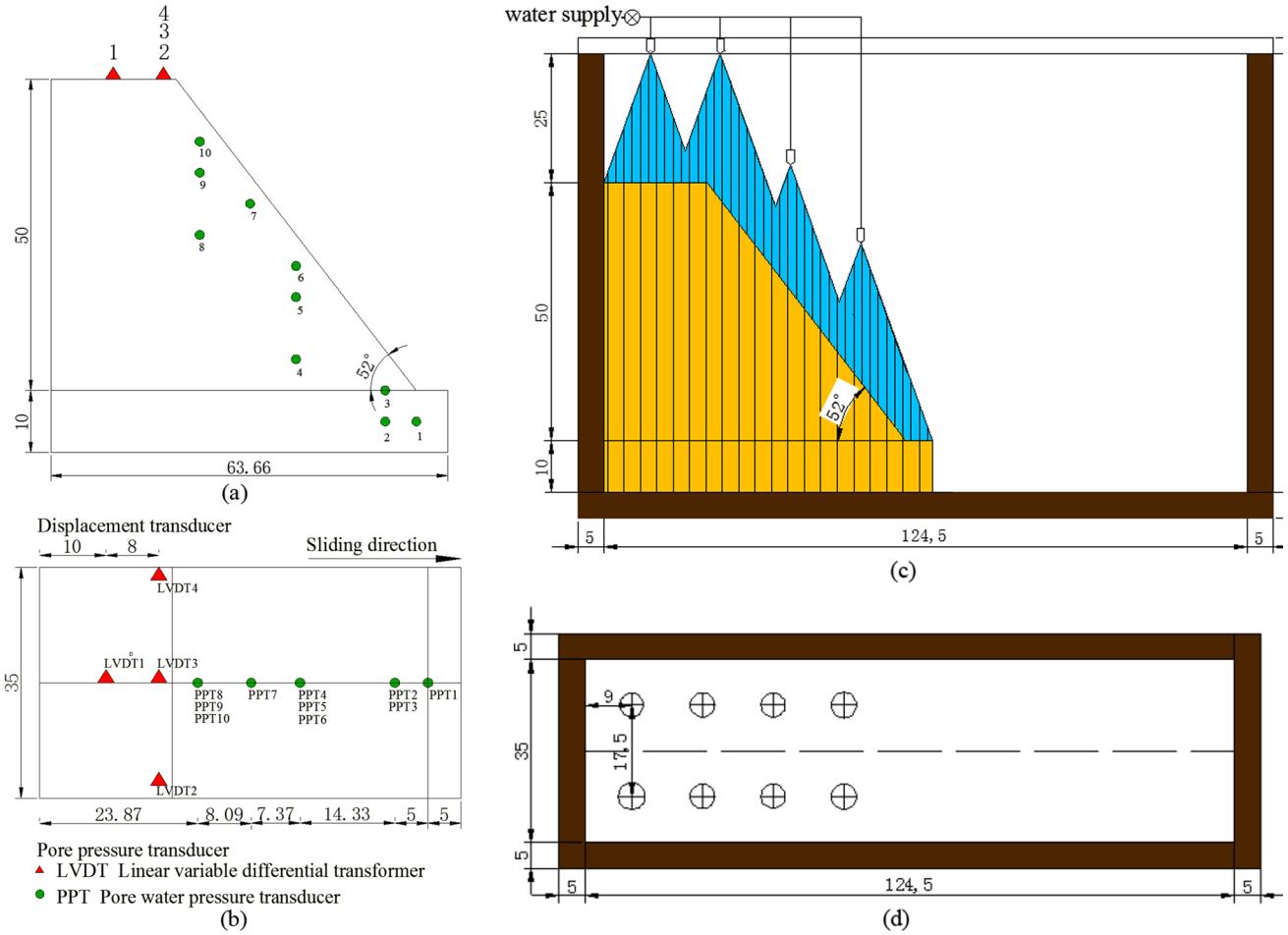

Fig. 5 Schematic diagram of model configuration (unit: cm) transducers **a** elevation view; **b** plane view; nozzles **c** elevation view; **d** plane view

is 500 mm (the ultimate height was 30 m in prototype when failure occurs).

The left, right and bottom boundaries of the model slope were set impermeable and mechanically fixed. Rainfall simulators were mounted with the strongbox to allow fixed rainfall intensity and duration to be applied and controlled during the test in flight. Any surface runoff was drained through holes at the bottom of the strongbox.

Model preparation

First, the wax seal of the intact loess soil block was opened and the completeness of soil sample was checked. Then, soil slope model of 52° was cut from the rectangular block. It should be noted that the evenness must be guaranteed. On the one hand, it is advantageous for soil surface and glass surface inosculating with each other; on the other hand, local stress concentration caused by the bad evenness could be eliminated, otherwise, soil rupture could be induced. Pore-water pressure transducers (PPT) were inserted through the pre-drilled holes of the model perpendicularly to the slope surface. The perspex wall and its opposite wall with silicon grease were put back to the strongbox to cover the soil slope. The final slope model is shown in Fig. 6. Figure 7 shows the typical setup of the centrifuge model package for rainfall test.

Instrumentation and input

During the model slope construction, miniature pore pressure transducers (PPT, DruckPDC 81) were installed at specified locations of the slope model as shown in Fig. 5a and b, for monitoring the response of pore-water pressure (PWP). The PPT locations were purposely chosen for measuring PWP changes in the model slope surface. Before installation, each PPT was subjected to a rigorous saturation and calibration procedures described by Zhou et al. (2006). Each PPT was able to measure PWP as low as − 75 kPa reliable without any sign of hysteresis and cavitation. It should be mentioned that, some PPTs in the test malfunctioned or desaturated during spinning up or during centrifuge test

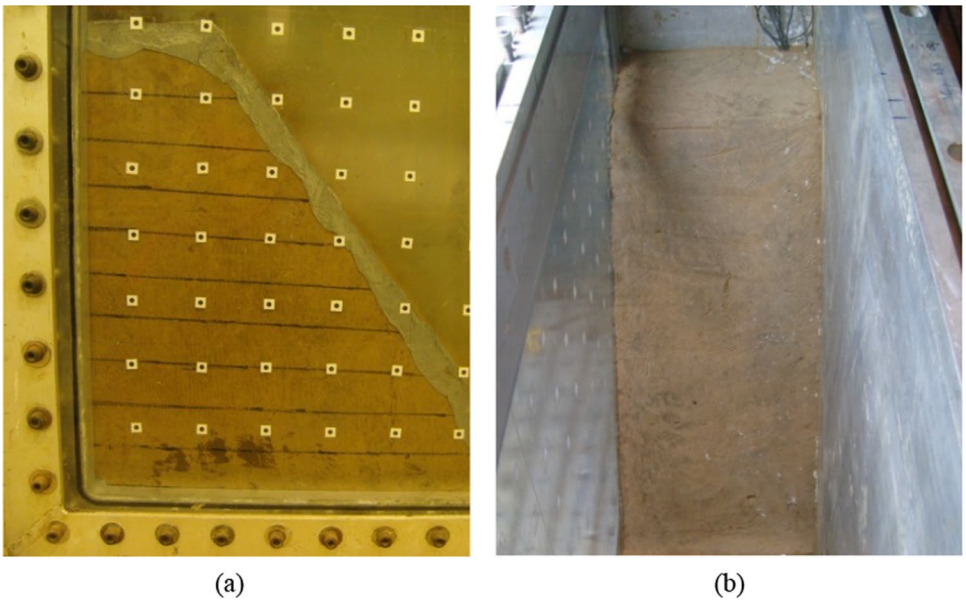

Fig. 6 Model preparation of intact loess slope **a** side view; **b** front view

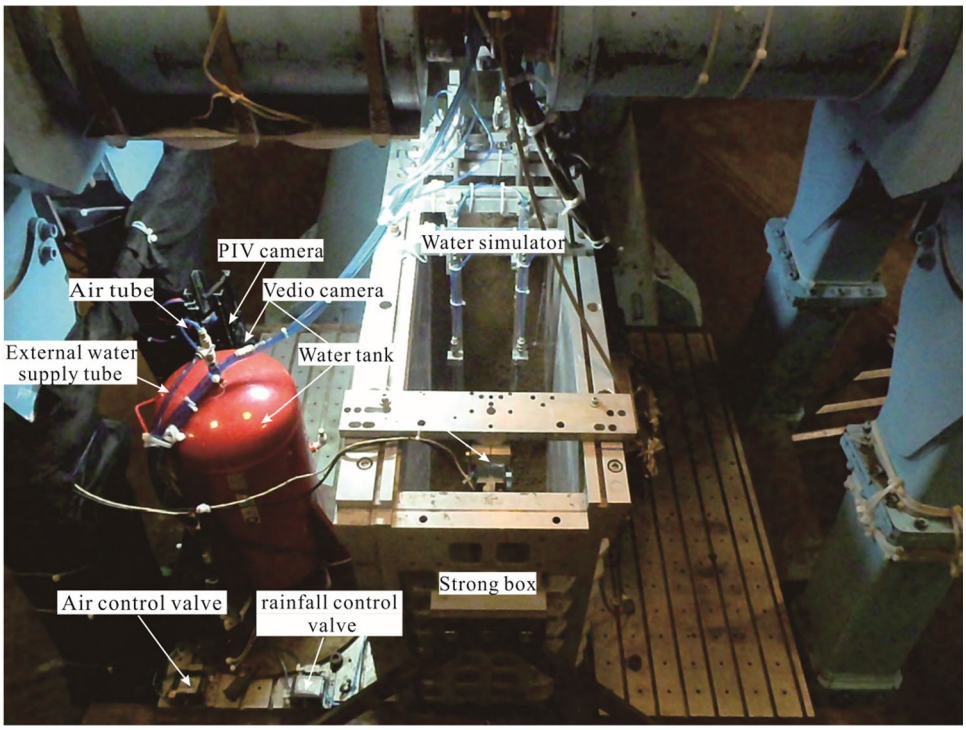

Fig. 7 Typical setup of the centrifuge model package for rainfall test

in-flight. Thus, only the PPTs that were working well are shown in the results.

Linear variable differential transformers (LVDT) were installed on the top of the slope at the designated locations as shown in Fig. 5a and b for monitoring the vertical displacement of the slope. Each LVDT was also subjected to a rigorous saturation and calibration procedures. The deformation of the loess slope have been measured by an image-based system of deformation measurement which combines the technologies of digital imaging, the image processing technique of particle velocimetry (PIV), and close-range photogrammetry (White et al. 2003). Using this technique, the deformation-failure process could be captured and evaluated quantitatively, Meanwhile, PIV operates on the image texture which avoids resorting to embedded target markers.

Results and analysis

PWP in slope

The hydrological response of the intact loess slope under heavy rainfall was shown in Fig. 8. Rainfall infiltration and pore-water pressure change are progressive; namely, PWP gradually increased with wetting front movement. The water content near slope foot increased faster than any other part of the slope as shown in Fig. 8. Before slope failure, the pore-water pressure increases after each rainfall and then stabilizes at a certain level. However, when the slope is damaged, the pore-water pressure shows a sharp increase or decrease (Fig. 8). Near 18,100 s, the transient responses of PWP at different position were opposite, such as the transient increase of PPT1, PPT3 but transient decrease of PPT2, PPT4 and PPT8. Transient response of PPT is the direct reflection of slope deformation and failure.

Vertical settlement of the slope

Figure 9 shows the vertical settlement of the slope. As shown in Figs. 8 and 9, the settlement increases with the increasing g level and rainfall infiltration. LVDT-1-3 show abnormal during the test, mainly due to the big settlement out of the scale range of LVDT. The settlement is limited before 20 g, after which it increases rapidly especially when g level reach 60 g (approaching 16,538 s). It should be noted that the settlement has a sharp increase after rainfall at 60 g, and then, the PWP shows sharp increase or sharp decrease (Fig. 8). The transient settlement reach 2.7 mm around, corresponding to 160 mm in prototype; and the total accumulative

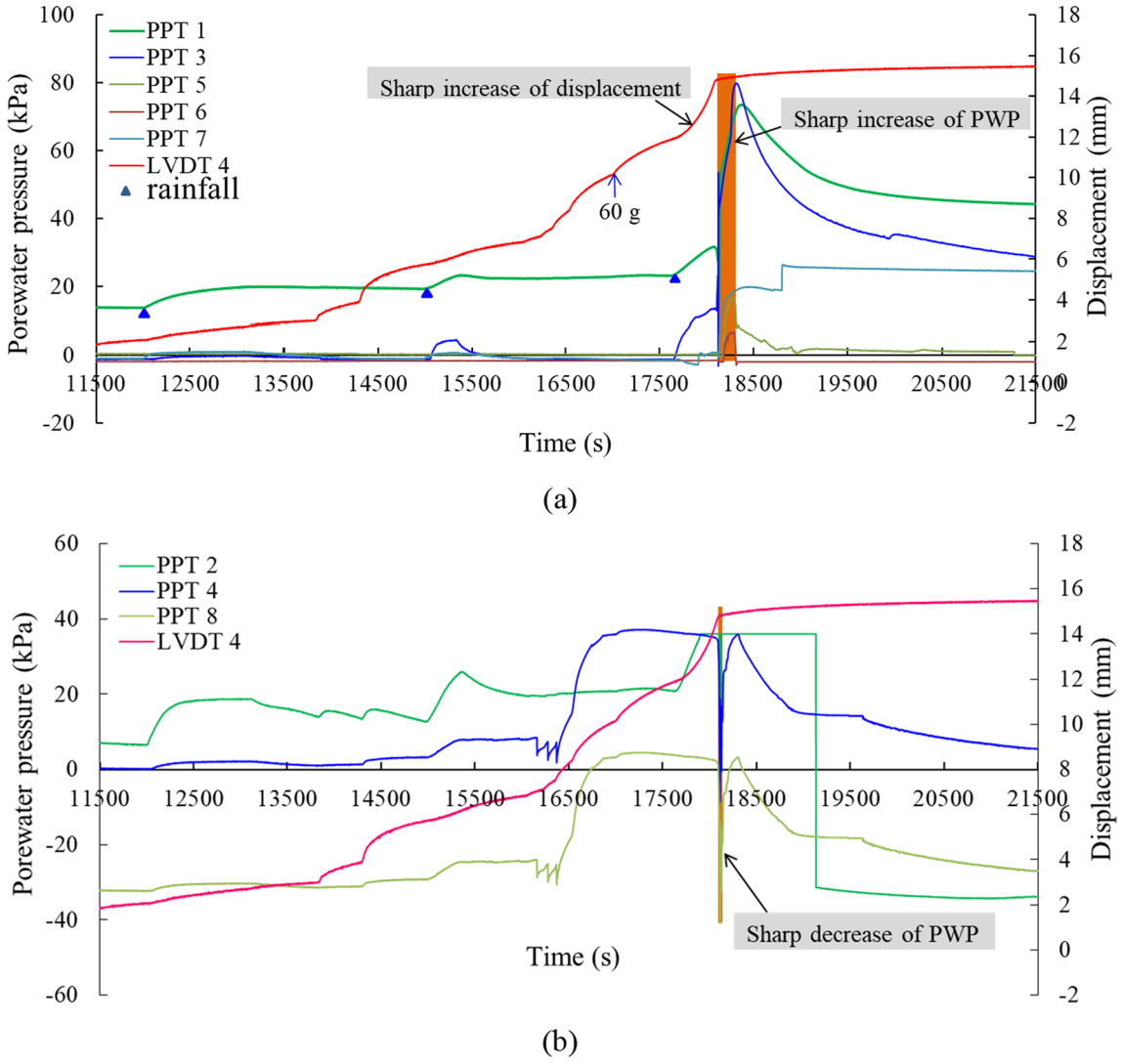

Fig. 8 PWP characteristics during rainfall **a** PPT near slope surface; **b** PPT relatively far from the slope surface

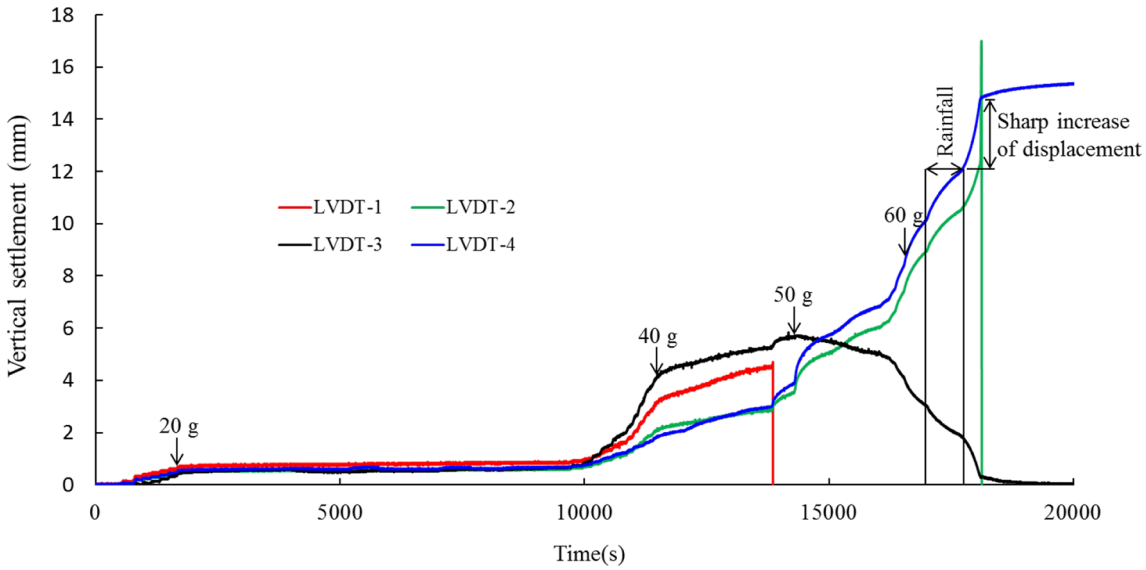

Fig. 9 Vertical settlement by LVDT

settlement reaches 15 mm, corresponding to 900 mm in prototype, slope failure happened.

Failure process and characteristics of slope

The special distribution of displacement vectors presented in Fig. 10 clearly demonstrates the progressive deformation-failure process and characteristics. As shown in Fig. 10, vertical settlement is evident and dominant during each g level increase, but the deformation by rainfall is very little before 60 g (not shown in Figures). It is consistent with the macroscopic displacement monitored by LVDT in Figs. 8 and 9. Evident displacements can be observed during the rainfall infiltration at 60 g, and the displacement vector has the tendency inclining to the slope surface and the slope toe, indicating the creep deformation toward the slope surface and the slope toe. With the creep movement outward and downward, thin tension crack appeared (Fig. 10d-2). Cracking should occur at the crown, but only the part we can see was depicted and the covered part by glass sealant was ignored. As shown in Fig. 10d-3–9, the crack developed and deepened with increasing length and aperture till slope failure happened. Cracking was closely related to the creep behavior of the slope. Furthermore, cracks accelerate rainfall infiltration and furthered the increase of the saturation, further decreasing the overall shear strength. So cracking at the crown was a key factor controlling slope failure.

The displacement vector map (Fig. 10) clearly demonstrated the movement direction of the soil and the big deformation and instability zone of the slope by rainfall. Meanwhile, it also well indicates the potential slide surface shown as yellow dotted in Fig. 10d-1–9. The potential sliding surface developed and deepened with rainfall till the sliding surface formed and the shallow slide-flow happened. The shallow failure depth is around 80–100 mm (as shown in Fig. 10d-8–9, corresponding to 4.8–6.0 m in prototype slope, belonging to shallow failure induced by rainfall in loess area. It is consistent with the sliding surface predicted by PWP. In addition, the upper deeper sliding surface is nearly straight which hints the deep shear movement of the soil.

Furthermore, the two potential sliding surfaces especially the shallow one is parallel to the slope surface, which was mainly affected by the wetting front during the rainfall. Ideally, the wetting front is a plane parallel to the slope surface if rainfall infiltration is uniform at the surface. Wetting front indicates the decrease of matric suction, i.e. an increase in pore-water pressure (Fig. 8). With the decreasing matric suction, slide-flow failure happened in the surface soil with two deeper potential sliding surfaces being clearly observed. The planar sliding is a marked feature of the landslide by rainfall-infiltration. Meanwhile, deeper sliding surface is characterized by straight sliding surface indicating creep shear movement and expending crack. So the slope failure synthesized the shallow slide-flow failure and deep creep-cracking.

In addition, several parallel tension cracks can be observed on the slope crown, mainly vertical downward. The abundant vertical joints in the loess, settlement crack in the settlement process and the tensile stress induced in the sliding process make the parallel cracks develop on the slope crown. It is important in the development of the high and steep head scarp. The height of the head scarp is about 10 m in prototype (about 160–170 mm in model scale).

Small holes of < 2 mm can be observed in slope crown, also along the surface of rupture at the head scarp, which

may be induced by rainfall infiltration. Some fissures and minor cracks are also well developed. On one hand, they are good for water infiltration; on the other hand, they can develop into major or large crack as an infiltration channel of advantage. In loess area, holes or cracks could be common along landslide boundary especially on the crown induced by tension stress or unload of the soil. With time going, the holes develop into a continuous big crack which is an infiltration channel of advantage. The holes promote the development of landslide; meanwhile, the landslides induce more holes development along the landslide boundary. The process will not stop until the landslide reaches a steady state condition.

Morphological characteristic s of the sliding surface

Closer examination was conducted on the horizontal and vertical distribution of the displacement of the slope at different positions from top to bottom (shown in Fig. 11). The results clearly indicated that the displacement decreased with increasing distance from the slope surface at a certain elevation. The displacement is very small and can be ignored at some positions. The position where displacement could be ignored is the potential sliding surface in the deeper soil far from slope surface. The position where the displacement has abrupt change could be taken as the potential easy-sliding surface at a shallower place. The surface soil has big deformation, which can't be captured by PIV, which is only designed for small deformation. So there are only several discrete displacement points in the large deformation area. Through the quantitative analysis of displacement at different positions along Y = 360 mm and Y = 250 mm as example (Fig. 12), it also indicates the larger deformation near the slope surface at each elevation. Meanwhile, the upper displacement is bigger than the lower part, and the vertical displacement (V-displacement) is bigger than the horizontal displacement (H-displacement) as shown in Fig. 13 taking X = 160 mm as example.

Failure patterns of slope

Figure 14 shows the failure patterns of the slope after test. During the intensive and continuous rainfall condition, creep sliding happened first at the foot of the slope, and then tension cracks developed at the slope crown. Two deeper continuous sliding surfaces can be observed clearly, which are mainly creepage sliding-tension type. It can be imaged that after the shallow failure, the deeper failure along the shear sliding plane would happen. So the multi-sliding retrogressive landslides would be dominant in the future till the slope reaches a new equilibrium state.

With the deformation accumulation and the sharp increase of displacement before failure, excess pore water pressure appears near the foot of the slope (Fig. 8). Sudden instability of the slope induced flow failure of the surficial soil at high speed. So the failure pattern of the slope in the model test is composed of shallow slide-flow and the deeper creep-cracking.

Discussion

PWP characteristics and flowslide failure

The opposite response of the PWP (Fig. 8) to the slope failure is mainly due to different behavior of soil contraction or unloading at the failure. The sharp decline of PWP (Fig. 8b) mainly indicated transient unload of the slope due to slide-flow of the outer surface, which is a strong proof of slop failure. Loess fabric and structure was broken with soil contraction followed, and then the sharp rise of PWP (Fig. 8a) appeared. Namely, the slope failure was followed by the sharp increase of excess pore water pressure. The phenomenon is common in the granular material, as stated by Iversion et al. (2000). Futhermore, the sharp increase of PWP may indicate the local liquefaction of loess occurred at the slope toe.

The abrupt vertical settlement monitored by LVDT (Fig. 9) is very critical for the formation of the excess pore water pressure, with the earlier accumulative deformation. Liquefaction happened after that and sliding transferred to flowing. Figure 8 certificates that the liquefaction is not the reason but the result of the deformation accumulation and big transient deformation (Eckersley 1990). According to Wen and Yan (2014), Jiang et al. (2014) and Liu et al. (2015), the breakage of cementation bonds is the essence of loess strength reduction and ultimate deformation and failure. During the rainfall-induced wetting process, the combined action of the decreasing matric suction, the progressive breakage of the cementation structure and the redistribution and migration of the soil grains leads to the deformation and even failure of loess slope. The breakage of the structure and cementation bonds dominates the deformation at the earlier stage, so the change of the pore water pressure is not evident; but the shear deformation dominates the later stage, during which soil contracts heavily. Then, the excess pore water pressure was produced in the local soil mass especially the soil near the slope toe. The water pressure was difficult to dissipate. Soil behavior changes from drainage shear to undrained shear. Liquefaction happened. It could be concluded that both the wetting-induced deformation and shear deformation contributed to the increase of the pore water pressure and leaded to the slide-flow movement of the loess slope; but the shear deformation dominants the last excess pore water pressure and the liquefaction.

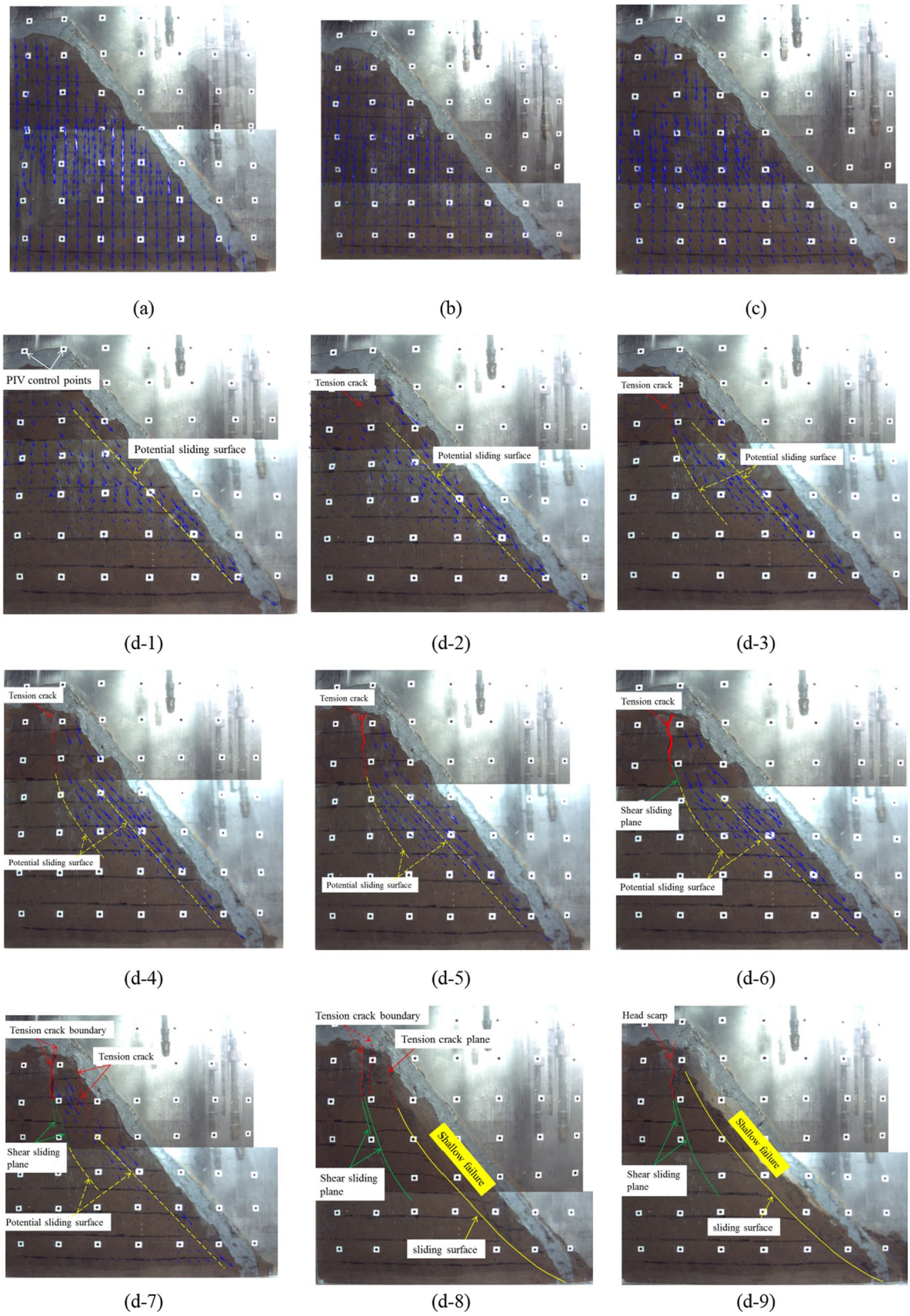
(a)
(b)
(c)
PIV control points
Potential sliding surface
(d-1)
Tension crack
Potential sliding surface
(d-2)
Tension crack
Potential sliding surface
(d-3)
Tension crack
Potential sliding surface
(d-4)
Tension crack
Potential sliding surface
(d-5)
Tension crack
Shear sliding plane
Potential sliding surface
(d-6)
Tension crack boundary
Tension crack
Shear sliding plane
Potential sliding surface
(d-7)
Tension crack boundary
Tension crack plane
Shear sliding plane
Shallow failure
sliding surface
(d-8)
Head scarp
Shear sliding plane
Shallow failure
sliding surface
(d-9)

◂**Fig. 10** Deformation-failure process and characteristic of the slope: displacement vector map during g level rising to **a** 40 g; **b** 50 g; **c** 60 g; rainfall at different time duration (h min s) at 60 g: (**d-1**) 00 00 00–00 06 51, (**d-2**) 00 06 51–00 07 51, (**d-3**) 00 07 51–00 08 03, (**d-4**) 00 08 03–00 08 15, (**d-5**) 00 08 15–00 08 21, (**d-6**) 00 08 21–00 08 27, (**d-7**) 00 08 27–00 08 32, (**d-8**) 00 08 32, (**d-9**) 00 08 32

Obviously, it is a complex chain process (Buscarnera and Prisco 2013): consisting of instability of loess slope, the transition from drained condition to undrained condition, the excess pore water pressure and eventually, catastrophic liquefaction of the loess. In fact, the chain process easily and widely exists in the soil slope failure as investigated by various researchers (Take et al. 2004; Ochiai et al. 2004; Buscarnera and Prisco (2013); Leng et al. 2018; Xu et al. 2012). Loess has an collapsive internal structure (Liu et al. 2015). Under long term rainfall infiltration, instability was induced, then the metastable structure collapsed and the material liquefied, triggering failure with high speed.

Planar sliding

Two parallel sliding surfaces could also be observed in the displacement distribution maps (Fig. 11). It also coincides with the displacement vector map (Fig. 10). Both the qualitative analysis (as shown in Fig. 10) and the quantitative

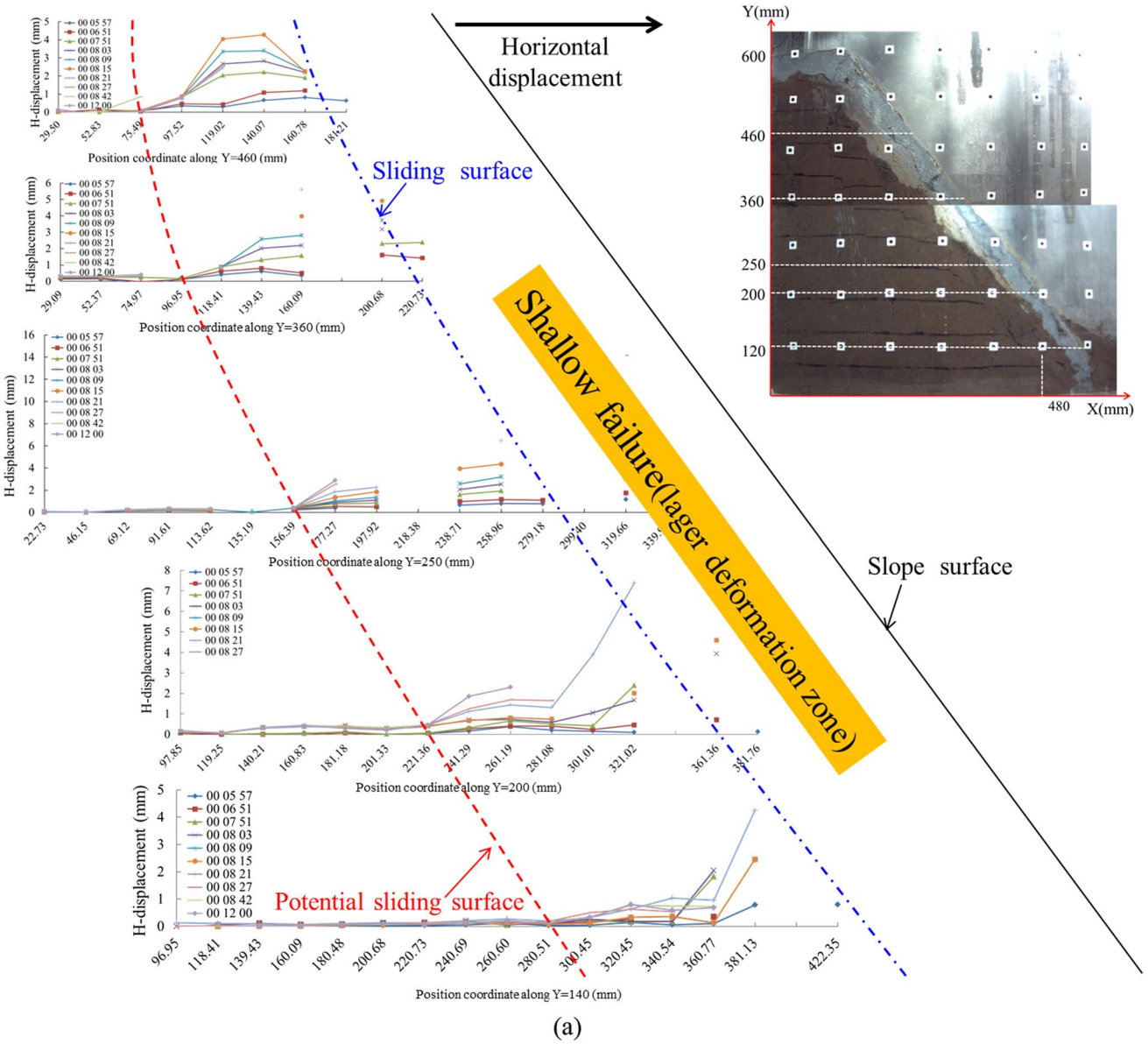

Fig. 11 Displacement distribution map **a** horizontal displacement; **b** vertical displacement

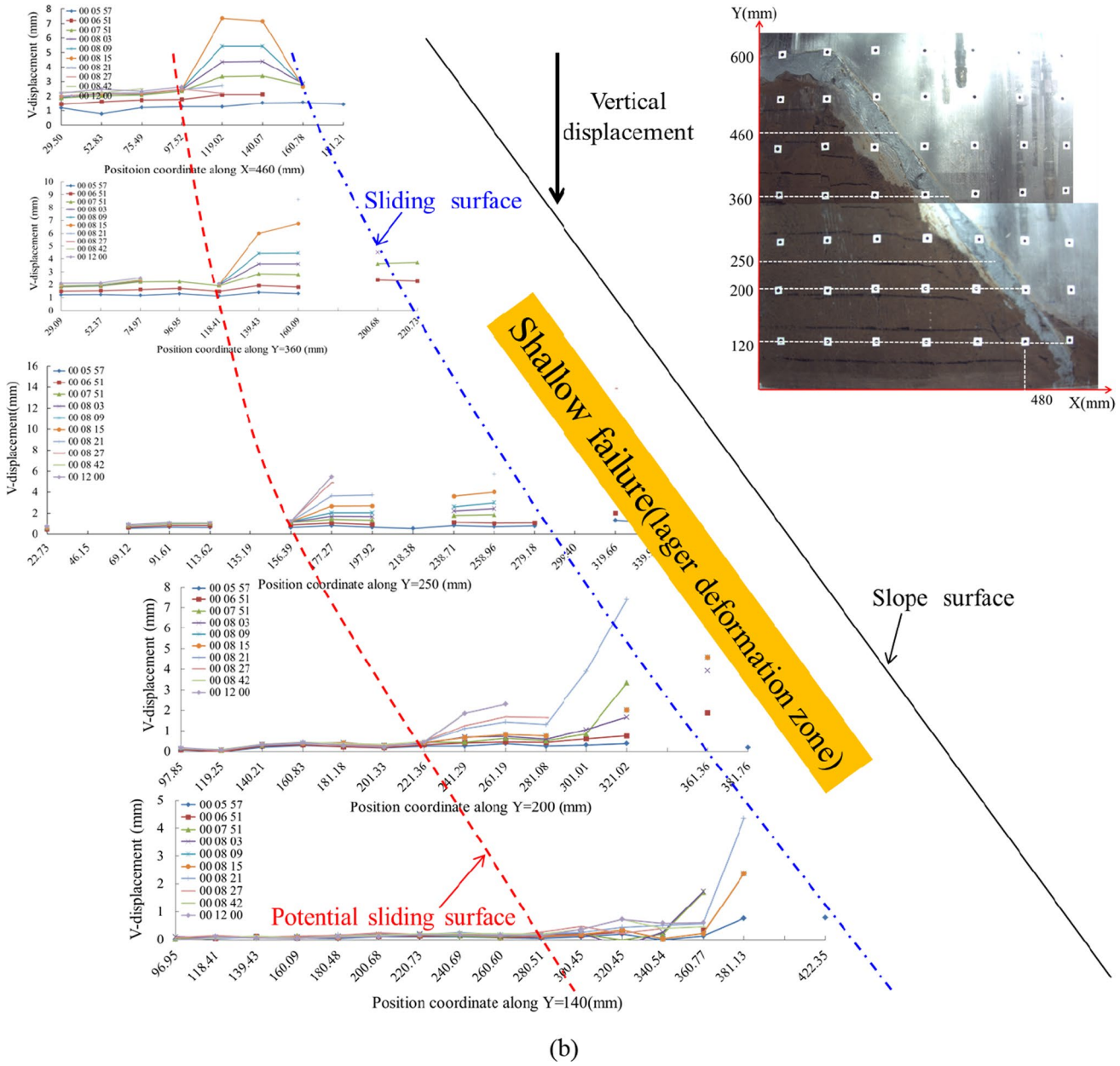

(b)

Fig. 11 (continued)

analysis (as shown in Fig. 11) certificate the planar sliding and failure of the slope by rainfall. In the centrifuge test on compacted loess slope, the planar sliding was also observed (Fig. 15). The compacted loess has the same geometry with the intact loess slope. Due to much less rainfall before instability than that in the intact loess slope, no subsequent liquefaction or flow occurred after the initial sliding. However, except the different depth of the sliding surfaces, the failure patterns are nearly the same. Both the intact and compacted loess slopes developed a shallow planar sliding surface (Fig. 15). The planar sliding surface differs a lot to the circular sliding surface in the gravitational soil landslide (Petterson 1955). The nearly planar sliding surface indicates a nearly uniform decrease of the matric suction along the wetting front, which is parallel to the slope surface by rainfall infiltration. The same phenomenon is also reported in the studies of rainfall-infiltration-induced dry ash dump landslide (Fourie et al. 1999), sand landslide (Mohammad et al. 2017; Wang et al. 2021b), and also loess landslides (Wu et al. 2017; Sun et al. 2021; Wang et al. 2021a).

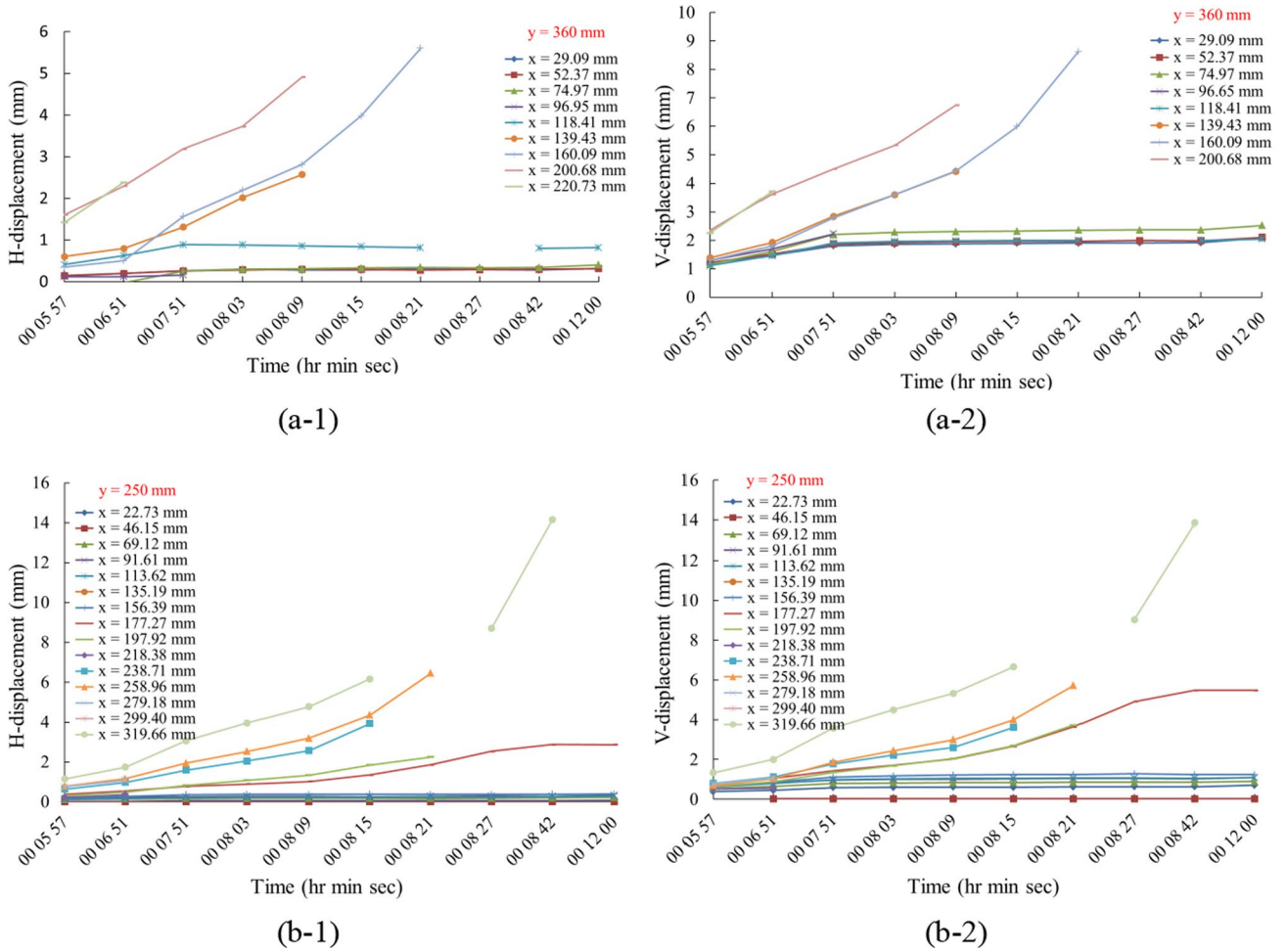

Fig. 12 Quantitative analysis of displacement with time at different positions along (**a-1–2**) Y = 360 mm; (**b-1–2**) Y = 250 mm

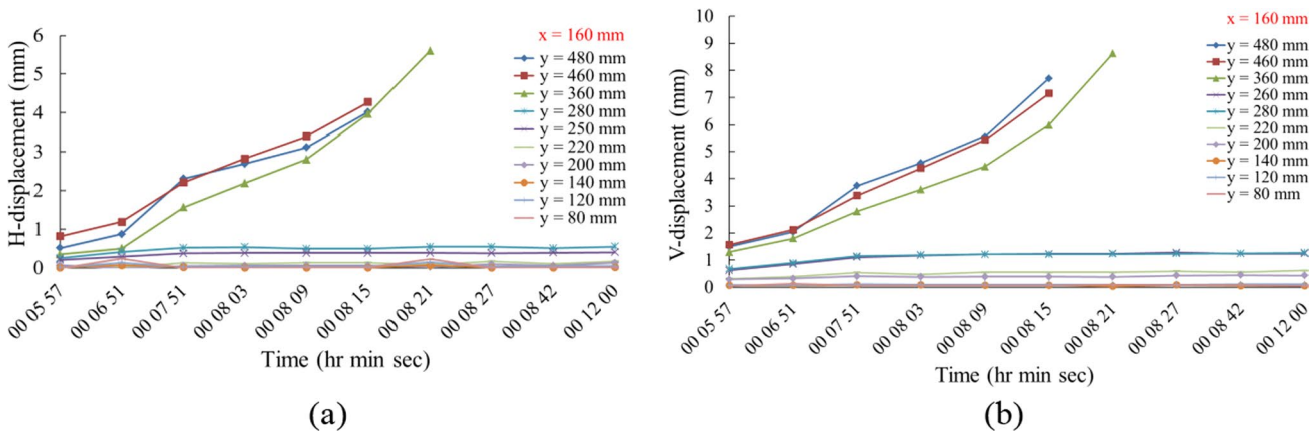

Fig. 13 Quantitative analysis of displacement at different positions along X = 160 mm

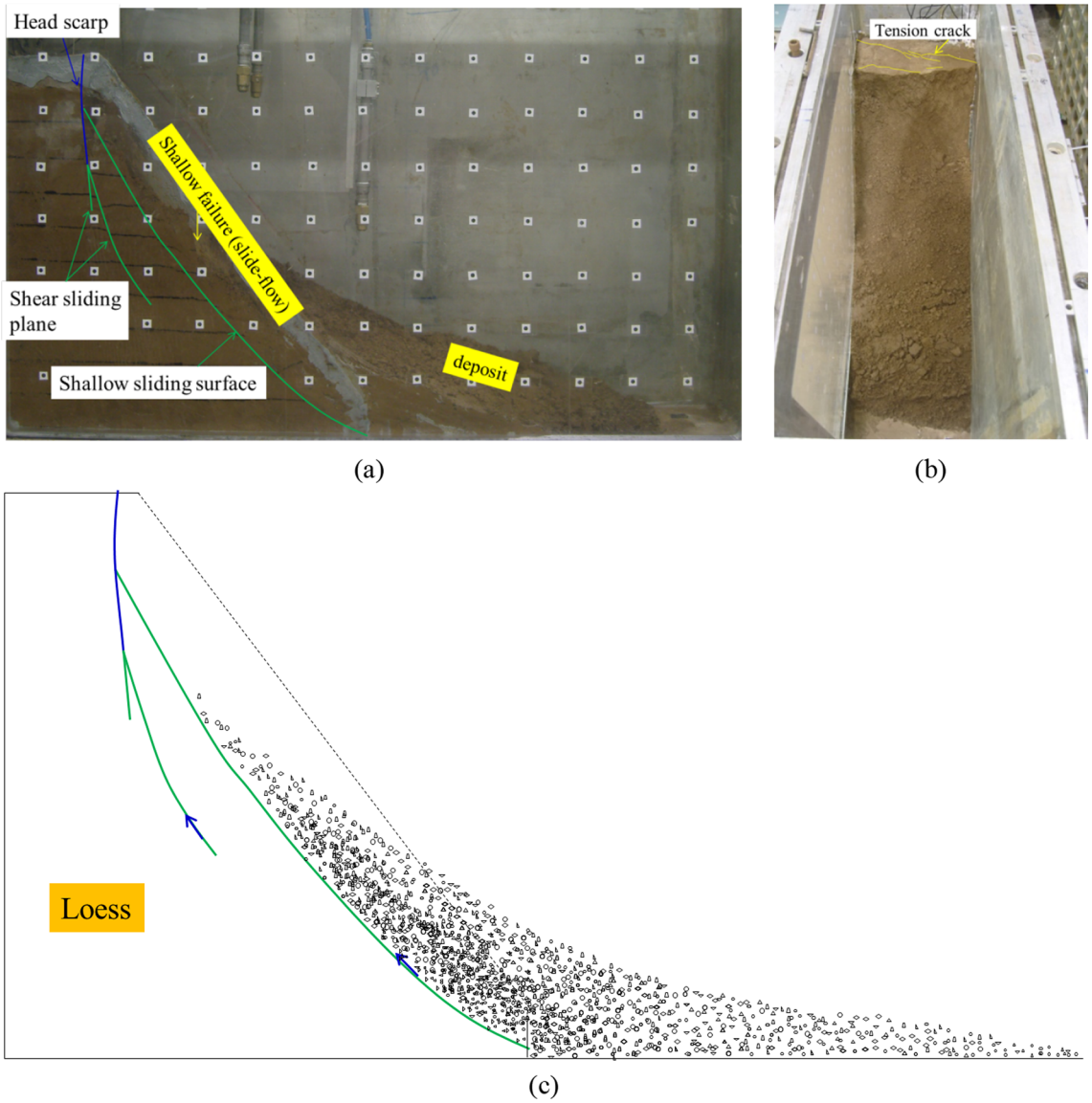

Fig. 14 Failure pattern of the slope **a** side view; **b** front view; **c** sketch of profile map

Matric suction plays an important role in the stability of unsaturated slopes (Lim et al. 1996; Fourie et al. 1999; Kim et al. 2004; Gu et al. 2019; wang et al. 2021b; Giuseppe and Marco 2013). The planar failure mode is mainly controlled by the wetting front or matric suction (Fourie et al. 1999; Wu et al. 2017; Mohammad et al. 2017; Wang et al. 2021a, b). Rainfall is evenly distributed along the slope surface, so the wetting front is nearly parallel to the slope surfaces especially at the initial stage which is determined by the conductivity. Matric suction decreases with the descending wetting front (Wang et al. 2021b; Zhao et al. 2021). The shear surface developed mainly in the superficial part of the slope, coinciding with the infiltration depth (Sun et al. 2021; Wang et al. 2021b). The failure mechanism is shallow, infinite-slope type (Mohammad et al. 2017). It was certificated by the simulation test using seepage/w by Wu et al. (2017) and Wang et al. (2021a), where it is obviously that the wetting front is parallel with the slope surface. Of course, due to the seepage, the wetting front near the toe part maybe thicker than the upper part (Wu et al. 2017). The final sliding surface may be not planar, which is also controlled by wetting front or matric suction. In recent years, the shallow planar landslides induced by intensified rainfall is reported frequently, such as the heavy rain-induced landslide in weathered granite (Dahal et al. 2009) and that in the loess region (Wang et al. 2015). They are all characterized by shallow translational sliding surfaces. According to the instrumented experiment in this study, the planar sliding surfaces are mainly controlled by matric suction or wetting front.

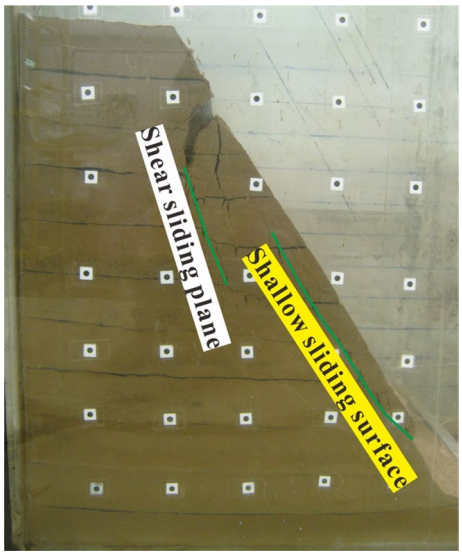

Fig. 15 Failure pattern of the compacted loess slope

Conclusions

An intact clayey loess slope model test by rainfall was carried out on a centrifuge, well instrumented with PPT, LVDT and PIV, to clarify the process of failure initiation and the progressive deformation-failure process of the loess slop. The following major conclusions are drawn from the analysis of results.

1. Rainfall-induced slope failure is characterized by shallow slide to flow and two sliding surfaces of creepage sliding-tension type. The accumulative deformation and the abrupt settlement before failure induced the excess pore water pressure, after which flow failure with high speed happened. The excess pore pressures were generated during rather than before movement, and liquefaction was a result of shear failure rather than the cause. The water pressure in both sides of the shallow sliding surface has opposite response to the slope failure, pressure increase or decrease due to soil contraction or unloading.
2. There exist two failure faces, which are characterized by planar sliding surfaces nearly parallel to the slope surface. Wetting front by rainfall is nearly parallel to the free surface. The planar sliding differs a lot to the circular sliding surface in the gravitational soil landslide.
3. LVDT data shows that the vertical settlement increase with the decreasing matric suction. PIV analysis results show that the displacement at the slope surface is bigger than that in the deeper position. Meanwhile, the upper displacement is bigger than the lower part, and the V-displacement is bigger than the H-displacement.
4. The failure pattern of rainfall-induced intact clay loess slope is composed of shallow slide-flow and the deeper creep-cracking. Cracks on the crown become infiltration channels of advantage, accelerating slope failure. Multi-sliding retrogressive landslides would be dominant in the future till the slope reaches a new equilibrium state.

Acknowledgements The authors express their sincere gratitude to Charles W. W. Ng, Qijie Ma, Dongri Song (HongKong University of Science and Technology, HKUST) for their help with the test during the research period.

Author contributions Changyu Liang and Shuren Wu conceived and designed the test. Changyu Liang contributed laboratory experimental steps and wrote the manuscript text. All authors obtained financial support for the project.

Funding This study was financially supported by the National Natural Science Foundation of China (Grant no. 41972301), the "Twelfth Five-Year" National Science and Technology Pillar Program (no. 2012BAK10B02) and the Scientific Research Fund of the Institute of Geomechanics, CAGS (no. DZLXJK201409).

Data availability The data that support the findings of this study are available from the corresponding author, upon reasonable request.

Declarations

Competing interests The authors declare no competing interests.

References

Buscarnera G, DI Prisco C (2013) Soil stability and flow slides in unsaturated shallow slopes: can saturated events trigger liquefaction process? Geotechnique 63(10):801–817

Cascini L, Cuomo S, Pastor M, Sacco C (2013) Modelling the post-failure stage of rainfall-induced landslides of the flow type. Can Geotech J 50(9):924–934

Chen W, Luo YS, Wu CP (2013) The laboratory model test study of loess slope under the artificial rainfall. China Rural Water Hydropower 5:100–104 (**In Chinese**)

Dahal RK, Hasegawa S, Nonomura A, Yamanaka M, Masuda T, Nishino K (2009) Failure characteristics of rainfall-induced shallow landslides in granite terrains of Shikoku Island of Japan. Environ Geol 56:1295–1310

Dijkstra TA, Rogers CSF, Smalley IJ, Derbyshire E, Jin LY, Meng XM (1994) The loess of north-central China: geotechnical properties and their relation to slope stability. Eng Geol 36:153–171

Eckersley D (1990) Instrumented laboratory flowslides. Géotechnique 40(3):489–502

Egeli I, Pulat HF (2011) Mechanism and modeling of shallow soil stability during high intensity and short duration rainfall. Sci Iran 18(6):1179–1187

Fourie AB, Rowe D, Blight GE (1999) The effect of infiltration on stability of the slopes of a dry ash dump. Geotechnique. 49(1):1–13

Gavin K, Xue JF (2008) A simple method to analyze infiltration into unsaturated soil slopes. Comput. Geotech. 35(2):223–230

GB/T50123 (2019) Standard for soil test method. Ministry of Construction, P.R. China (**In Chinese**)

Giuseppe S, Marco VN (2013) Unsaturated soil mechanics in rainfall-induced flow landslides. Eng Geol 165(24):105–132
Gu TF, Zhang MS, Wang JD, Wang CX, Xu YJ, Wang X (2019) The effect of irrigation on slope stability in the Heifangtai Platform, Gansu Province. China Eng Geol 248:346–356
Hakro MR, Harahap ISH (2015) Laboratory experiments on rainfall-induced flowslide from pore pressure and moisture measurements. Nat Hazards Earth Syst Sci Discuss 3:1575–1613
Huang JP, Ran JJ, Ji MX (2014) Preliminary analysis of the flood disaster over the arid and semi-arid regions in China. Acta Meteorol Sin 72(6):1096–1107 (**In Chinese**)
Iversion RM, Reid ME, Iversion NR, LaHusen RG, Logan M, Mann JE, Brien DL (2000) Acute sensitivity of landslide rates to initial soil porosity. Science 290(5491):513–519
Jiang MJ, Zhang FG, Hu H, Cui YJ, Peng JB (2014) Structural characterization of natural loess and remolded loess under triaxial tests. Eng Geo 181:249–260
Kim J, Jeong S, Park S, Sharma J (2004) Influence of rainfall-induced wetting on the stability of slopes in weathered soils. Eng Geol 75:251–262
Leng YQ, Peng JB, Wang QY, Meng ZJ, Huang WL (2018) A fluidized landslide occurred in the loess plateau: a study on loess landslide in South Jingyang tableland. Eng Geol 236:129–136
Li WC, Lee LM, Cai H, Li HJ, Dai FC, Wang ML (2013) Combined roles of saturated permeability and rainfall characteristics on surficial failure of homogeneous soil slope. Eng Geol 153:105–113
Li P, Li TL, Fu YK, Chang W, Hou XK, Yan L (2014) In-situ observation on regularities of rainfall infiltration in loess. J Cent South Univ (sci Technol) 45(10):3551–3560 (**In Chinese**)
Liang CY, Cao CS, Wu SR (2018) Hydraulic-mechanical properties of loess and its behavior when subjected to infiltration-induced wetting. Bull Eng Geol Environ 77:385–397
Lim TT, Rahardjo H, Chang MF, Fredlund DG (1996) Effect of rainfall on matric suctions in a residual soil slope. Can Geotech J 33:618–628
Ling H, Ling HI (2012) Centrifuge model simulations of rainfall-induced slope instability. J Geotech Geoenviron Eng 138(9):1151–1157
Ling HI, Wu MH, Leshchinsky D, Leshchinsky B (2008) Centrifuge modeling of slope instability. J Geotech Geoenviron Eng 135(6):758–767
Liu Z, Liu FY, Ma FL, Wang M, Bai XH, Zheng YL, Zhang GP (2015) Collapsibility, composition, and microstructure of a loess in China. Can Geotech J 53(4):673–686
Mohammad A, Nejan H, Nabi KT (2017) Rainfall-triggered landslides in an unsaturated soil: a laboratory flume study. Environ Earth Sci 76:735
Ng CWW, Shi Q (1998) A numerical investigation of the stability of unsaturated soil slopes subjected to transient seepage. Comput Geotech 22(1):1–28
Ng CWW, Pang YW (2000) Influence of stress state on soil-water characteristics and slope stability. J Geotech Geoenviron. 126(2):157–166
Ochiai H, Okada Y, Furuya G, Okura Y, Matsui T, Sammori T, Terajima T, Sassa K (2004) A fluidized landslide on a natural slope by artificial rainfall. Landslides 1(3):211–219
Oh S, Lu N (2015) Slope stability analysis under unsaturated conditions: case studies of rainfall-induced failure of cut slopes. Eng Geol 184:96–103
Peng JB, Lin HC, Wang QY, Zhuang JQ, Cheng YX, Zhu ZH (2014) The critical issues and creative concepts in mitigation research of loess geological hazards. J Eng Geol 22(4):684–691 (**In Chinese**)
Petterson KE (1955) The early history of circular sliding surfaces. Geotechnique 5(4):275–296
Qi TJ, Zhao Y, Meng XM, Chen G, Dijkstra T (2021) AI-Based Susceptibility Analysis of Shallow Landslides Induced by Heavy Rainfall in Tianshui. China. Remote Sens. 13(9):1819
Sorbino G, Nicotera MV (2013) Unsaturated soil mechanics in rainfall-induced flow landslides. Eng Geol 165(15):105–132
Sun P, Wang HJ, Wang G, Li RJ, Zhang Z, Huo XT (2021) Field model experiments and numerical analysis of rainfall-induced shallow loess landslides. Eng Geol 295:106411
Take WA, Bolton MD (2002) An atmospheric chamber for the investigation of the effect of seasonal moisture change on clay slopes. Proceedings of the international conference on physical modelling in geotechnics—ICPMG'02, pp 765–770
Take WA, Bolton MD, Wong PCP, Yeung FJ (2004) Evaluation of landslide triggering mechanism in model fill slopes. Landslides 1(3):173–184
Taylor RN (1995) Geotechnical centrifuge technology. Blackie Academic & professional, London
Tohari A, Nishigaki M, Komatsu M (2007) Laboratory rainfall-induced slope failure with moisture content measurement. J Geotech Geoenviron Eng 133(5):575–587
Tu XB, Kwong AKL, Dai FC, Tham LG, Min H (2009) Field monitoring of rainfall infiltration in a loess slope and analysis of failure mechanism of rainfall-induced landslides. Eng Geol 105(1–2):134–150
Wang FH, Li JC, Tian WP (2009) Test on rainfall filtration in loess slope. J chang'an Univ (nat Sci Edn) 29(4):20–24 (**In Chinese**)
Wang R, Zhang G, Zhang JM (2010) Centrifuge modeling of clay slope with montmorillonite weak layer weak layer under rainfall conditions. Appl Clay Sci 50(3):386–394
Wang GL, Li TL, Xing XL (2015) Research on loess flow-slides induce by rainfall in July 2013 in Yan'an, NW China. Environ Earth Sci 73:7933–7944
Wang HJ, Sun P, Wang G, Wu LZ (2021a) Experimental and numerical study of shallow loess slope failure induced by irrigation. CATENA 206:205548
Wang S, Idinger G, Wu W (2021b) Centrifuge modeling of rainfall-induced slope failure in variably saturated soil. Acta Geotech 16:2899–2916
Wen BP, Yan YJ (2014) Influence of structure on shear characteristics of the unsaturated loess in Lanzhou. China. Eng. Geo 168:46–58
White DJ, Take WA, Bolton MD (2003) Soil deformation measurement using particle image velocimetry (PIV) and photogrammetry. Géotechnique 53:619–631
Wu SR, Wang T, Shi JS, Shi L, Xin P (2013) A review of engineering landslide prevention and control. Geol Bull China 32(12):1871–1880 (**In Chinese**)
Wu LZ, Zhou Y, Sun P, Shi JS, Liu GG, Bai LY (2017) Laboratory characterization of rainfall-induced loess slope failure. CATENA 150:1–8
Xin P, Wu SR, Shi JS, Wang T, Shi L (2015) Comment on progress in problems and countermeasure on Mudflow induce by rainfall. Geol Rev 61(3):485–493
Xu L, Dai FC, Gong QM, Tham LG, Min H (2012) Irrigation-induced loess flow failure in Heifangtai Platform North-West China. Environ Earth Sci 66:1707–1713
Xu L, Li P, Li TL, Wang AD, Zhang YG, Liang Y, Zhao JF (2013) In-situ test research on regularities of water migration in loess. Rock Soil Mech 34(5):1331–1339 (**In Chinese**)
Zhang G, Wang R, Qian JY, Zhang JM, Qian JM (2012) Effect study of cracks on behavior of soil slope under rainfall conditions. Soils Fund 52(4):634–643
Zhao ZQ, Dai FC, Min H, Tu XB (2021) Field infiltration of artificial irrigation into thick loess. Eng Geol 294:106388

Zhou ZBR, Take WA, Ng CWW (2006) A Case Study in tensiometer interpretation: centrifuge modelling of unsaturated slope behaviour. In Unsaturated Soils 2:2300–2311